



# An ultrasensitive non-enzymatic electrochemical cholesterol sensor based on copper foam/CuO/Pt/ p-phenylenediamine molecularly imprinted polymer

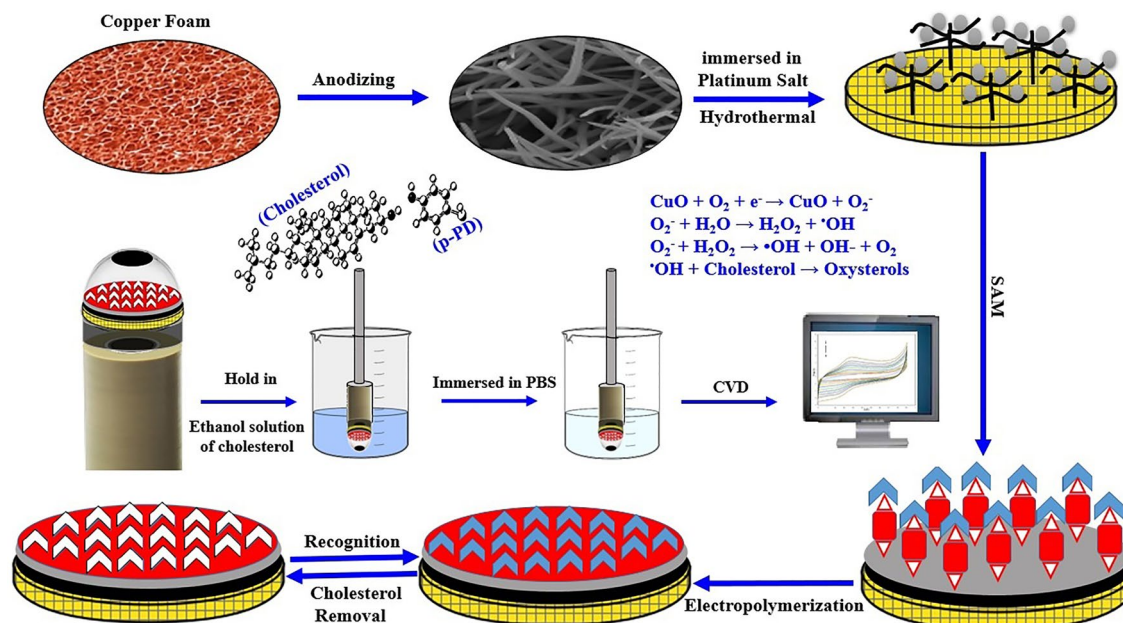
Milad Eghbali<sup>1,2</sup> · Farshad Kheiri<sup>3</sup> · Mohammad Sirousazar<sup>1</sup> · Elham Jannatdoust<sup>1</sup> · Arash Afghan<sup>3</sup>

Received: 9 February 2023 / Accepted: 25 April 2023 / Published online: 15 May 2023  
© The Author(s), under exclusive licence to Springer Nature B.V. 2023

## Abstract

A novel amperometric non-enzymatic biosensor was developed for cholesterol (CHO) detection based on electropolymerized para-phenylenediamine (p-PD) monomer as a molecularly imprinted polymer (MIP) on the copper foam (CF) modified with platinum (Pt) and copper oxide (CuO) dual-core nanohybrid (CuO/Pt) which was attached on the GCE using carbon glue. UV–Vis spectrophotometry, X-ray diffraction (XRD), grazing XRD (GXR), energy-dispersive X-ray spectroscopy (EDX), field-emission scanning electron microscopy (FESEM), and Fourier-transform infrared (FT-IR) spectroscopy were utilized to characterize the prepared nanocomposites. The non-enzymatic CHO biosensor showed a detection limit of 0.035  $\mu\text{M}$ , a sensitivity of 157.85  $\mu\text{A}\mu\text{M}^{-1}\text{cm}^{-2}$ , and a linear range of 0.4–6  $\mu\text{M}$ . Density functional theory (DFT) was used to select the most suitable functional monomer for synthesizing MIP. For the first time, the effect of sensor loading time in cholesterol solution was investigated on the rise of direct oxidation current. Herein, CF/CuO/Pt/CHO-MIP nanocomposite was employed as a selective and suitable catalyst in CHO oxidation due to their high conductivity, large specific surface area, and good electrocatalytic performance. The superior catalytic activity and selectivity introduce the CuO/Pt nanohybrids on the CF surface as a promising nanomaterial for applications in the direct detection of CHO.

## Graphical abstract



**Keywords** MIP · DFT · Cholesterol · Nanocomposite · Biosensor

## 1 Introduction

Cholesterol (CHO) is one of the most well-known lipids as high blood CHO levels cause cardiovascular diseases such as high blood pressure, coronary heart disease, and atherosclerosis [1]. Therefore, the development of a fast, selective, and sensitive CHO detection method with low cost and good stability is highly welcome [2]. In recent years, amperometric electrochemical CHO biosensors have attracted a lot of attention due to their cost-effectiveness, high selectivity, and simplicity [3]. Numerous recent studies have addressed the fabrication of enzyme-based CHO biosensors [4]. The unstable nature of enzymes, however, reduces their performance during the stabilization process as their performance is under the influence of toxic chemicals, temperature, and pH [5]. Moreover, enzyme-based sensors do not have proper reproducibility and need further improvements. To overcome the limitations, non-enzymatic CHO sensors have been extensively explored due to their low cost, facile fabrication, reproducibility, and optimal stability [6]. In this type of sensors, different nanomaterials and their hybrids can be used as a suitable and selective catalyst instead of the enzymes used in CHO oxidation [7]. Among the various nanomaterials such as Au nanoparticles (NPs) [8], copper (I) sulfide nanoplates [6], and Ag NPs [9], Pt NPs could be an ideal candidate for non-enzymatic CHO sensors owing to their large specific surface area, high conductivity, and good electrocatalytic performance [10].

In general, fabrication of non-enzymatic electrochemical sensors requires the integrated design of electrocatalysts with conductive substrates [11, 12]. Among the various synthesis methods, electrochemical anodizing has been considered due to its single-stage synthesis, cost-effectiveness, functional diversity, and direct connection (wireless) between metal oxide nanostructures and conductive metal substrate [13]. Anodized cupric oxide (CuO) nanoclusters are a promising candidate for the fabrication of electrochemical non-enzymatic CHO biosensors due to the possibility of direct etching from the conductive copper substrate and the appropriate electrocatalytic activity, leading to direct electron transfer with low potential [14]. In recent years, numerous studies have been conducted to increase the selectivity of non-enzymatic CHO sensors in the presence of complex matrices. In this regard, molecularly imprinted polymers (MIP) can be employed as a recognition element in sensors [15]. Various methods (chemical bonding, molecular self-assembly, electropolymerization, and photochemistry) have been developed for the synthesis of MIPs [16]. These methods differ from the other in terms of the type of target molecule binding to the functional monomer and the polymer binding sites. Electropolymerization is more

practical in preparation of MIP film on electrodes. Studies have reported successful use of the electropolymerization to prepare electroactive and Electro-inactive polymers on a variety of conductive surfaces, including platinum, indium tin oxide, carbon, oxidized metals, stainless steel, and zinc (Zn). The success of MIP synthesis depends on the selection of the optimal functional monomer; as the functional monomers can create the greatest interaction with the target molecule to achieve high selectivity and rebinding capacity. In conventional methods, the optimal monomer is selected based on empirical experiments which would be tedious and time-consuming. Therefore, density functional theory (DFT) was used to select the polymer composition for the molecular imprinting process [1, 17].

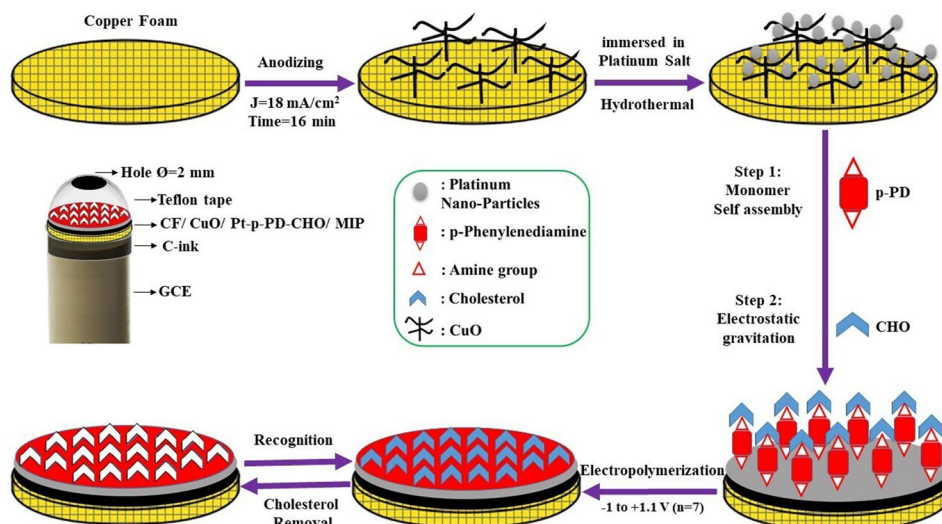
This study reports the development of a novel amperometric non-enzymatic direct oxidation CHO biosensor based on the electropolymerization of the p-PD monomer as an MIP on the Pt and CuO dual-core nanocomposite (CF/CuO/Pt/MIP) which was prepared on the surface of CF through hydrothermal and anodization methods and then attached on the GCE using carbon glue. Density functional theory (DFT) was utilized to select the most suitable functional monomer for the synthesis of MIP. For the first time, the effect of sensor retention time in cholesterol solution was explored on increasing direct oxidation current.

## 2 Experimental

### 2.1 Synthesis of Pt nanoparticles on CF electrode modified with CuO nanoclusters (CF/CuO/Pt)

All chemicals were obtained from Merck. Copper foam was from Alfa Aesar co (USA). A scanning electron micrograph (SEM) was recorded for the further characterization and morphology of the proposed surface modifier using a Philips xl-30 electron microscope operated at 25 kV. Characterization was investigated using a Fourier transform infrared spectroscopy (FTIR) instrument (thermo Nicolet nexus® 670, USA) in the transmittance mode between  $400\text{ cm}^{-1}$  and  $4000\text{ cm}^{-1}$ . UV-vis spectroscopy measurement was performed on (2601, Ray Leigh) UVvis spectrophotometer in aqueous solution (1 mg/3ml). Electrochemical experiments were performed using Autolab PGSTAT30 Potentiostat/Galvanostat equipped with a frequency response analyzer (FRA4.9) and controlled by General Purpose Electrochemical System (GPES4.9) software (Eco Chemie, Utrecht, Netherlands). All the details of the synthesis process of CF/CuO/Pt nanocomposite are provided in the supplementary information. All the details of the synthesis process of CF/

**Scheme 1** The procedure for preparing CF/CuO/Pt/CHO-MIP



CuO/Pt nanocomposite are provided in the supplementary information.

## 2.2 Computational methods

The Gaussian 09 package program was used for DFT calculations. The electron stability energies ( $\Delta E$ ) of the structures were calculated using the DFT scheme at the B3LYP level with G + 31–6 basis set. Computational details are briefly described in the supplemental information.

## 2.3 Self-assembly of p-PD and CHO on the CF/CuO/Pt

The CF/CuO/Pt nanocomposite was immersed in an ethanolic solution containing 5 mM p-PD for 24 h. Afterward, the resulting CF/CuO/Pt was washed with ethanol and deionized water to remove non-bonded (unabsorbed) p-Pd ions from the surface. Then, the p-PD-modified CF/CuO/Pt was immersed in an ethanol solution containing 1 mM CHO for 24 h. Finally, the resulting CF/CuO/Pt-p-PD-CHO was washed with ethanol. Due to the presence of two  $-\text{NH}_2$  functional groups in the p-PD structure, it can bind to Pt nanoparticles on the one side and the CHO molecule on the other.

## 2.4 Synthesis of MIP by electropolymerization method (CF/CuO/Pt/CHO-MIP)

As can be seen in Scheme 1, to synthesize the CHO-MIP, the CF/CuO/Pt-p-PD-CHO was immersed in an ethanol solution containing 5 mM CHO, 10 mM p-PD and 10 mM  $\text{NaClO}_4$ . Electropolymerization was performed by applying seven consecutive cycles in the potential range of  $-1$

to  $+1.1$  V (Vs. Ag/AgCl) at a scan rate of 50 mV/s. After electropolymerization, the modified electrode was immersed in an ethanol solution containing 0.5 mol/L HCl and a stable potential of  $-0.1$  V was applied for 40 s to remove CHO molecules from the MIP and create selectable sites to attach on the GCE using carbon glue. The surface area of the electrode was kept constant using Teflon adhesive. A control polymer was synthesized as molecular non-imprinted polymer (NIP) to perform comparative tests and confirm the selectivity of synthesized MIP. The synthesis steps of this polymer are the same as those of CHO-MIP, except that CHO was not used in the polymerization solution.

## 3 Results and discussion

### 3.1 Characterization and evaluation of synthesis of CuO nanoclusters on CF surface (CF/CuO)

FESEM images of anodized CF surface (Fig. 1A–E) illustrate arrays of CuO nanoclusters with a large surface area which uniformly covered the macro porous surface of the CF. At higher magnifications, the diameter of the nanoclusters varies from 30.21 to 72.42 nm. The FESEM images show a uniform distribution of CuO nanoclusters on the CF surface, which ultimately leads to an increase in the surface area of CF, providing a suitable substrate for the uniform growth of Pt NPs and preventing their accumulation in the subsequent stages. EDX analysis was also performed to evaluate the purity of the CF surface (Fig. 1F). As can be seen, oxygen (O) and copper (Cu) are the only two constituents of anodized CF. By examining the purity of these components (oxygen with a purity of 47.46 and copper with a purity of

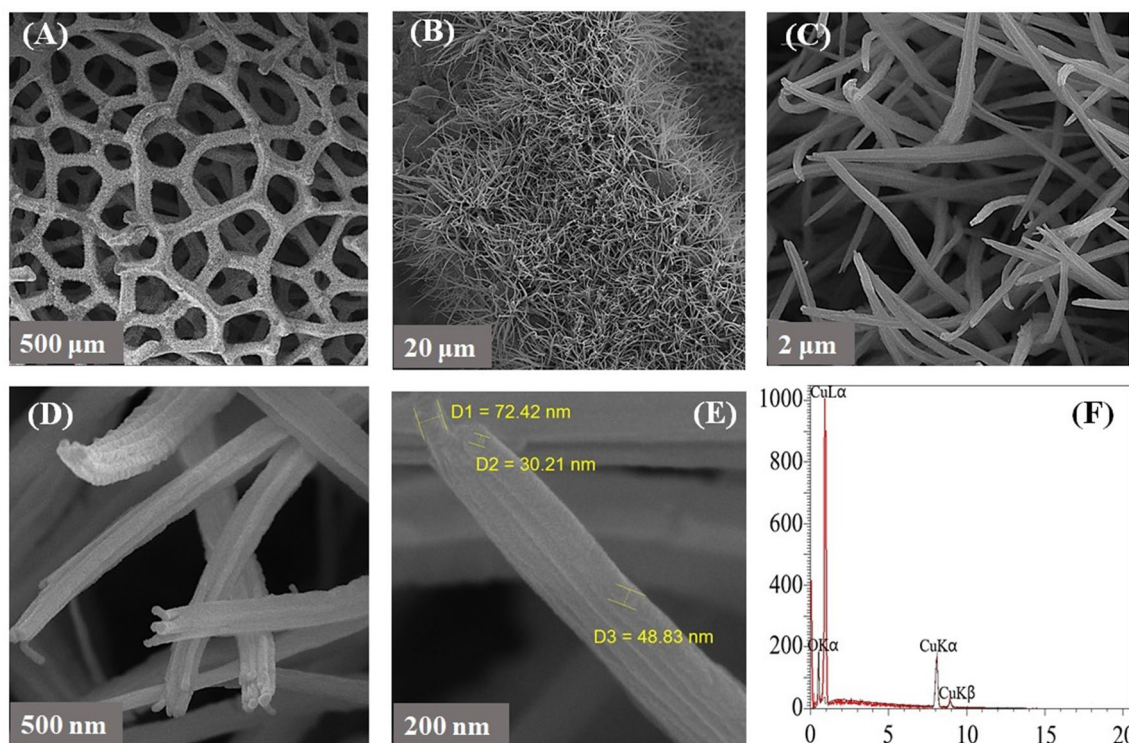


**Fig. 1** A–E FESEM image with different magnifications of CF electrode modified with CuO nanoclusters, F EDX analysis of modified CF electrode with CuO nanoclusters

52.54), it can be concluded that CuO is formed on the surface of CF without any other impurities. In all experiments, the surface area was 0.031 cm<sup>2</sup>.

### 3.2 Characterization and evaluation of synthesis of Pt nanoparticles on CF electrode modified with CuO nanoclusters (CF/CuO/Pt)

Figures 2A–D shows FESEM images of the CF/CuO/Pt surface at different magnifications. As seen, the use of a three-dimensional substrate of ultra-thin CuO nanoclusters led to the uniform growth of Pt nanoparticles without agglomeration on the surface of the CF. This property will enhance the electrocatalytic activity of the nanocomposite. The FESEM images also demonstrate the spherical morphology of the synthesized Pt with an average diameter of 19.59–51.33 nm. EDX analysis was also used to investigate the purity and elemental distribution of the electrode surface after the growth of Pt nanoparticles (Fig. 2E). As seen, the EDX diagram only shows the constituent elements of the CF/CuO/Pt nanocomposite, namely Pt, Cu and O. No impurities were detected in the prepared nanocomposite. According to Fig. 2F and in accordance with the FESEM results, Pt NPs are evenly distributed on the electrode surface. The pattern observed in Fig. 2G shows

four severe grazing XRD diffraction peaks at  $2\theta = 41, 43, 50.5, \text{ and } 74^\circ$ , representing CuPt (006), Cu (111), Cu (200) and Cu (220) planes, respectively. Several other diffraction peaks at  $2\theta = 35.5, 38.5, 40, 45.5, \text{ and } 48^\circ$  also suggest the presence of CuO (002), CuO (111), Pt (111), Pt (200), and CuPt (404) planes, respectively. The density of diffraction Pt (200) is less than the card number 01-087-0640 and has half wider peak, since Pt could be reduced and absorb hydrogen under hydrothermal conditions.

### 3.3 Selection of the most suitable functional monomer

According to Table S1 and Fig S2, the stability of the complexes formed in the gas phase between each of the monomers and CHO molecule follows the following order: (2-Merc) > (p-Hyd) > (p-PD) > (p-Amin). On the other hand, the influence of the solvent was also investigated as the electropolymerization operation was performed in the liquid phase and the solvent can affect the molecular imprinting process and its efficiency. The polarizable continuum model (PCM) was implemented for molecular complex systems to estimate the interaction energies between CHO and each monomer dissolved in a specific solvent. The results are presented in Table 1. As seen, the presence of ethanol affects the bond

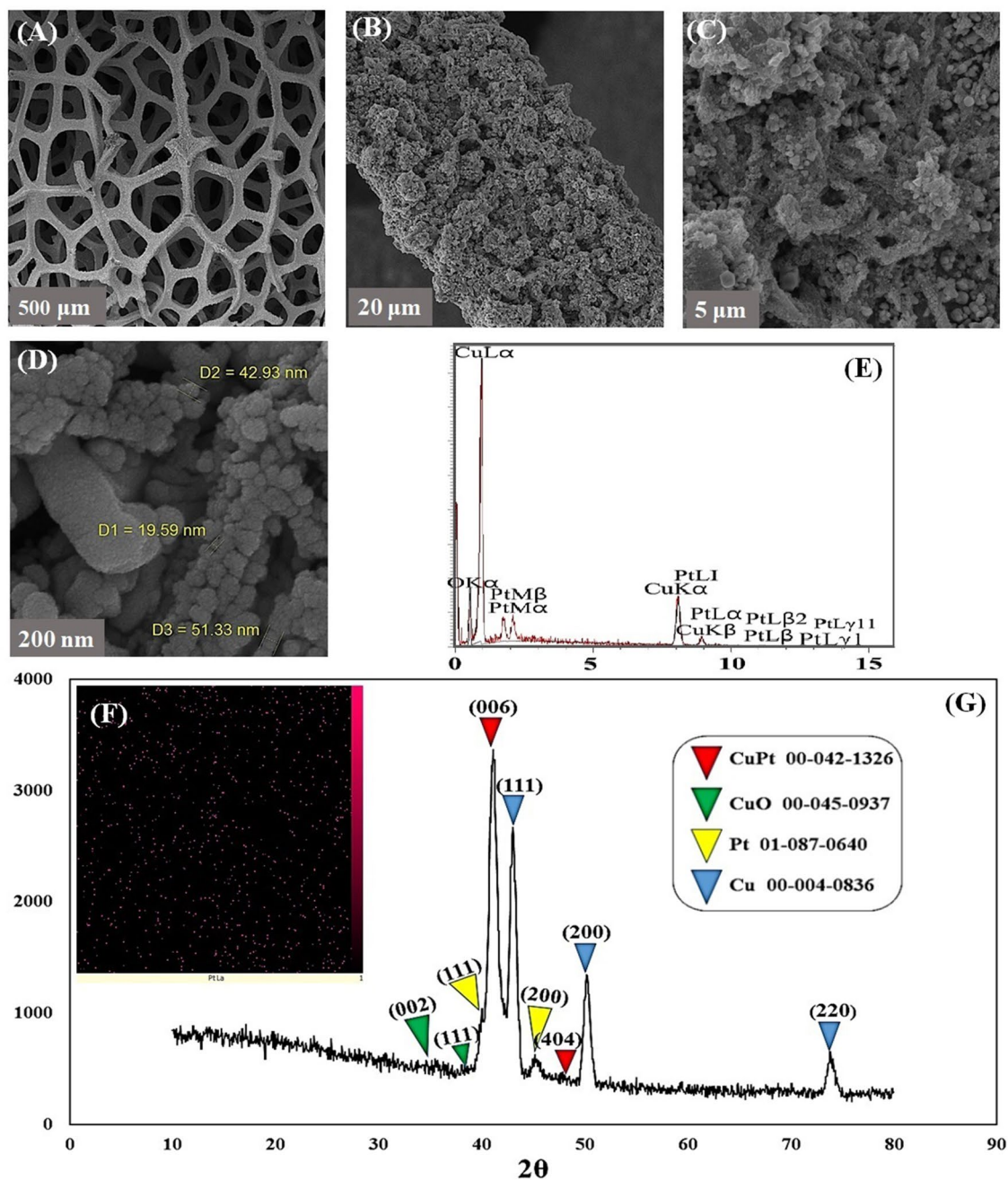


**Fig. 2** A–D FESEM image, E EDX analysis and F Distribution map of Pt nanoparticles on CF/CuO/Pt electrode G grazing XRD diagram of CF/CuO/Pt electrode

**Table 1** Calculated bond energies for the monomer-CHO complex in ethanol solvent

Molecules	E (Hartree)	$\Delta E$ (Hartree)	$\Delta E$ (kJ/mol)
p-Phen- CHO	- 1474.4770357	- 0.0098187	- 6.1613
p-Hyd- CHO	- 1837.1262634	0.0032411	2.03382
p-Amin-CHO	- 1817.2906653	- 0.0066463	- 4.17061
2-Merc-CHO	- 1909.521962	- 0.011924	- 7.482429

energy between the monomer and CHO. The stability ranking of the complexes in the presence of ethanol is different from that of the gas phase. Accordingly, the stability of the complexes formed in the ethanol solvent between each of the monomers and the CHO molecule has the following order: (2-Merc) > (p-PD) > (p-Amin) > (p-Hyd). The absolute value of the bond energies for 2-Merc and p-PD are 7.482429 and 6.1613, respectively. Regarding to the proximity of the

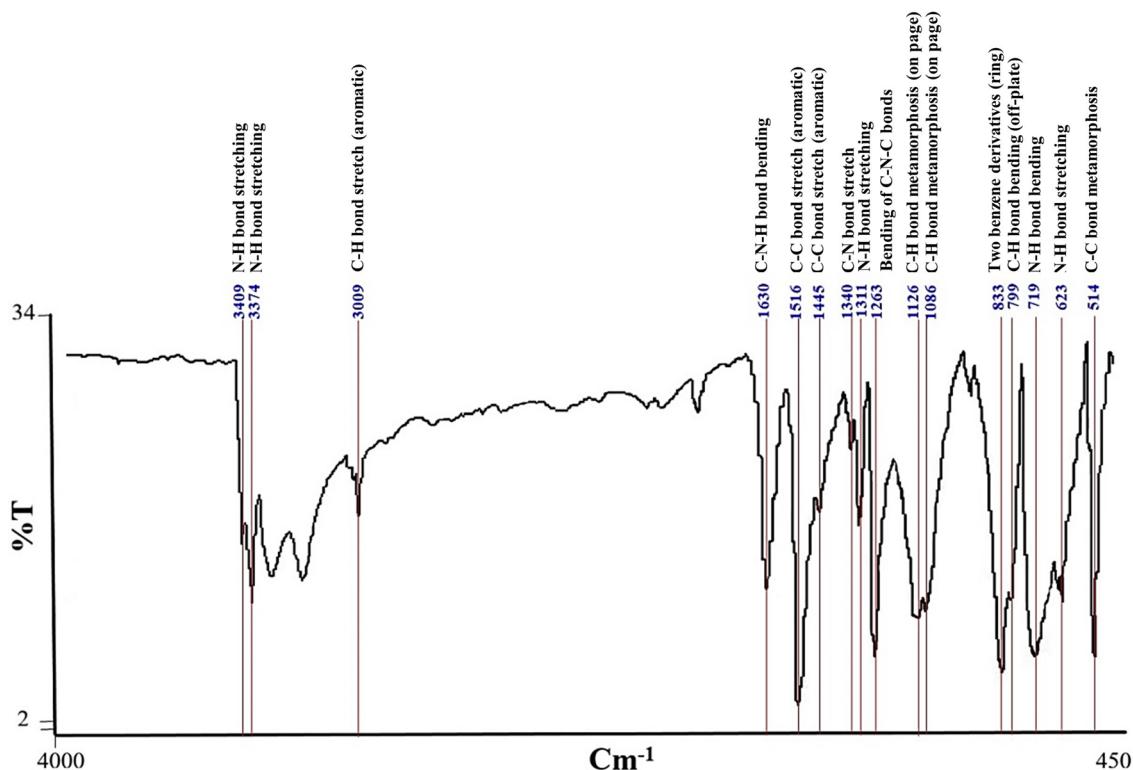


Fig. 3 FT-IR spectrum of p-PD on CF/CuO/Pt/GCE

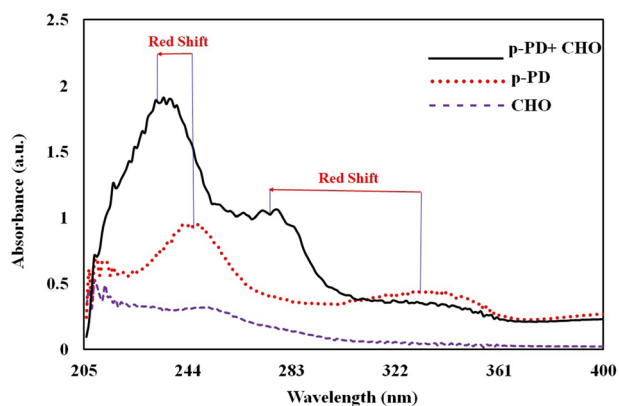


Fig. 4 UV-VIS spectrum of CHO, p-PD and CHO-p-PD bond

bonding energies of these two monomers and the greater stability of p-PD, the p-PD was employed in the synthesis of MIP.

### 3.4 Evaluation of synthesis of p-PD on CF/CuO/Pt nanocomposite by FT-IR

The FT-IR spectrum of p-PD synthesized by the electropolymerization process on CF/CuO/Pt/GCE is shown in Fig. 3. The following vibration peaks can be observed:

- N–H vibrations

The p-PD structure has two functional groups of  $\text{-NH}_2$  in the para position. Vibration peaks related to N–H traction emerged at  $3409$  and  $3374$   $\text{cm}^{-1}$ . The N–H bending peak also appeared in  $798$   $\text{cm}^{-1}$  while the vibration peak related to C–N–H bending was observed at  $1630$   $\text{cm}^{-1}$ .

- C–H vibrations

Existing aromatic structures indicate the presence of C–H stretching vibrations in the range of  $3000$ – $3100$   $\text{cm}^{-1}$ . In this sample, the C–H peak appeared at  $3009$   $\text{cm}^{-1}$ . In-plane bending vibration peaks can be also observed at  $1126$  and  $1086$   $\text{cm}^{-1}$ . The peak related to off-plane bending of C–H can be detected at  $719$   $\text{cm}^{-1}$ .

- C–C vibrations

In this sample, stretching vibrations of the C–C bond can be observed at  $1516$  and  $1445$   $\text{cm}^{-1}$ . However, a C–C deformation peak was observed in this sample at  $514$   $\text{cm}^{-1}$ .

- C–N vibrations

The vibration peak corresponding to the C–N stretching vibration emerged at  $1340$   $\text{cm}^{-1}$ . The peak due to C–N–C bending vibrations can be observed at  $1263$   $\text{cm}^{-1}$ .

- Ring vibrations

The peak due to the combination of two benzene derivatives in the p-PD structure appeared at  $833\text{ cm}^{-1}$  [18].

### 3.5 Evaluation of CHO and p-PD monomer bond using UV–VIS spectroscopy

Figure 4 shows the UV–vis spectrum of CHO, p-PD, and CHO-p-PD in ethanol solvent. The peak of CHO does not appear in this wavelength range; moreover, p-PD shows two common absorption peaks at  $\sim 245$  and  $337\text{ nm}$ , which is consistent with previous reports [6]. The first absorption peak at  $\sim 237\text{ nm}$  can be assigned to the  $\pi\text{-}\pi^*$  bond of the p-PD benzene ring; while the second absorption peak at  $\sim 278\text{ nm}$  is related to the p- $\pi$  conjugate bond through sharing electrons between  $\text{NH}_2$  and the benzene ring. The CHO-p-PD bond spectrum also shows two absorption peaks at  $\sim 237$  and  $278\text{ nm}$ . Based on Fig. 4, the link between CHO and the p-PD functional groups doubled the density of absorption as well as the red shift (displacement of the absorption peak to shorter wavelengths); suggesting the proper binding of CHO to p-PD.

### 3.6 Investigation of the conductivity of different layers of CuO/Pt/MIP

The ability of a surface to conduct electricity decreases with increasing electrical resistance ( $R$ ). Therefore, electrical conductivity is defined as the inverse of resistance, and in other words, the current density is directly related to the amount of electrical conductivity of the surface. The electrical conductivities of different layers of the electrode are briefly described in the Supplemental Information. The cyclic voltammograms of electrodes modified with CuO, CuO/Pt and CuO/Pt/MIP were examined as shown in Fig. S3.

### 3.7 The effect of CHO loading duration in MIP on biosensor response

In the present work, considering the use of MIP technology in the manufacturing of the electrode, it should be considered that after polymerization and selection of selectable sites on the modified electrode surface, CHO molecules are attached to these sites by bonding and

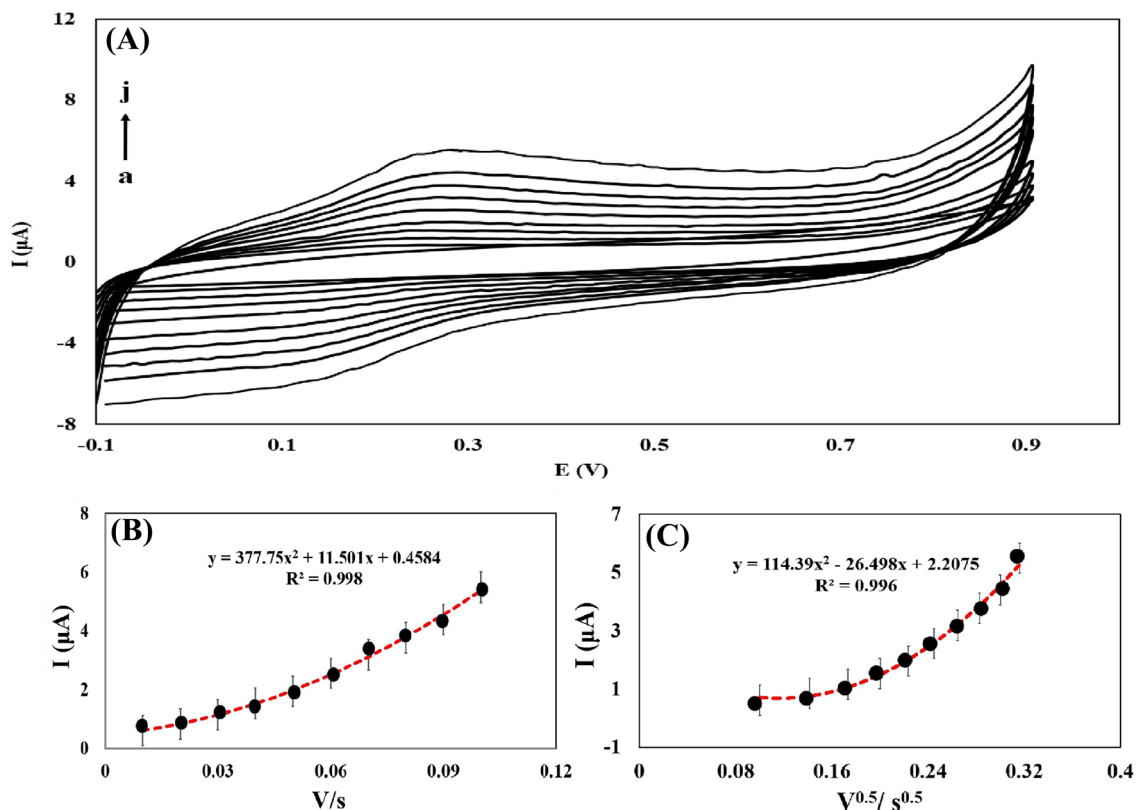


**Fig. 5** A The electrochemical behavior of modified biosensor at a CHO concentration of  $0.8\text{ }\mu\text{M}$  and different scan rates (10, 20, 30, 40, 50, 60, 70, 80, 90, and 100 corresponding to (a) to (j), respectively) B

The anodic peak current of the modified electrode vs. scan rates at a CHO concentration of  $0.8\text{ }\mu\text{M}$  of C The current of the CHO oxidation at the surface of the modified electrode

complex formation. Therefore, based on the mentioned process, reviewing and optimizing the time required to load CHO molecules on the surface of the modified electrode can be effective in the accuracy and precision of the biosensor designed to detect CHO. Therefore, to evaluate the optimal duration for the loading of CHO molecules within the polymer sites, a certain volume of the stock CHO solution (0.8  $\mu\text{M}$ ) was poured into 10 ml of ethanol. Then, the modified electrode was examined at different time intervals from 20 to 240 s. First, the modified electrode was placed in an ethanolic solution containing a certain concentration of CHO for 20 s. Then, the modified electrode was examined in the electrolyte solution (ethanol and  $\text{NaClO}_4$ ) with the potential range of  $-0.1$  to  $+0.9$  V and a scanning rate of 50 mV/s. The mentioned process was then examined for up to 240 s at different times. Fig. S4 shows the ratio of current density to different loading times. According to this figure, by increasing the loading time of CHO up to 160 s, the obtained current density increases uniformly compared to the initial times. Therefore, in the present work, based on the resulting diagrams, a time of 160 s was chosen as the optimal time for optimal loading of CHO molecules within the MIP structure.

### 3.8 Biosensor behavior at different scan rates

Figure 5A shows the current vs. the applied potential while Fig. 5B illustrates the current density vs the scan rates. The presence of cathodic and anodic peaks indicates the reversibility of this process. Figure 5B suggests a linear relationship for the electro-oxidation activity of CHO. The electrode surface coverage ( $\Gamma^*$ ) can be calculated using the slope of this diagram and Laviron theory (Eq. 1).

$$I_p = \left( \frac{n^2 F^2}{4RT} \right) \cdot V \cdot A \cdot \Gamma^* \quad (1)$$

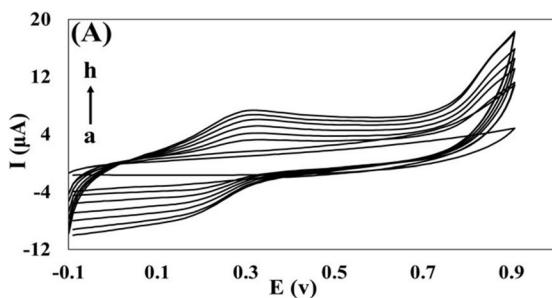


**Fig. 6 A** Cyclic voltammogram of CF/CuO/Pt/CHO-MIP designed biosensor in the presence of different concentrations of CHO; curves (a) to (h) respectively correspond to 0, 0.4, 1.2, 2.0, 2.8, 3.6, 4.4 and

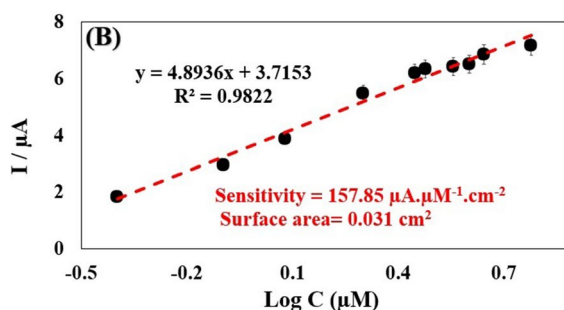
In this equation,  $A$  shows the surface area of the electrode ( $\text{cm}^2$ ),  $V$  is the scan rate,  $F$  denotes the Faraday constant,  $n$  is the number of electrons exchanged in the redox process ( $n = 1$ ).  $I_p$  represents the density of the anodic current.  $R$  and  $T$  also respectively show the global constant of gases and ambient temperature (K). The electrode surface coverage was calculated to be  $4.3 \times 10^{-9}$  mol/ $\text{cm}^2$ . Figure 5C shows the current density of the CHO oxidation at the surface of the modified electrode. The CHO diffusion coefficient can be calculated based on the Randles–Sevcik equation (Eq. 2).

$$I_p = (2.68 \times 10^5) n^{1.5} \cdot A \cdot C_0 \cdot v^{0.5} \cdot D_0^{0.5} \quad (2)$$

In this equation,  $V$  is the potential scanning rate (V/s),  $C_0$  represents the concentration (mol/ $\text{cm}^3$ ),  $A$  is the electrode surface area ( $\text{cm}^2$ ),  $I_p$  denotes the current density (A) and  $n$  is the number of electrons exchanged. Based on this equation, the diffusion coefficient of CHO at a concentration of 0.8  $\mu\text{M}$  was calculated to be  $1.49 \times 10^{-5}$   $\text{cm}^2/\text{s}$ .

### 3.9 Direct electrochemical oxidation of CHO at different concentrations

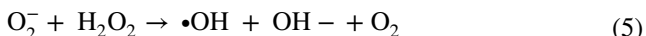
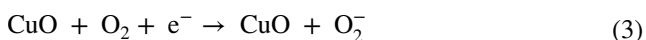
Figure 6A shows the cyclic voltammograms of the designed biosensor at different concentrations. Accordingly, the current density peak of CHO oxidation increases by enhancing the CHO concentration. This indicates the electrooxidation process of CHO at the designed nano-catalyst surface (CuO/Pt). As the CHO concentration increased, more CHO molecules were loaded on selective MIP sites and the desired nano-catalyst surface, incrementing the current density peak of CHO oxidation. Due to the strong adsorption of  $\text{O}_2$  to CuO, oxygen can be converted into  $\text{O}_2^-$  and then react with  $\text{H}_2\text{O}$  to produce  $\text{H}_2\text{O}_2$  and hydroxyl radicals (Eqs. 3, 4, and 5). Hydroxyl radicals



**6.0  $\mu\text{M}$  B** CHO biosensor calibration curve in the concentration range of 0.4 to 6.0  $\mu\text{M}$



thus initiated the cholesterol auto-oxidation to produce oxysterols (Eq. 6) [14].



$$\text{LOD} = 3 \frac{SD}{m} \quad (6)$$

Platinum NPs on the CF/CuO/Pt nanocomposite can enhance the electrical conductivity of the sensor, thus facilitating the cholesterol oxidation. The linear range of the designed biosensor was from 0.4 to 6  $\mu\text{M}$ . As can be seen in Fig. 6B the sensitivity of the biosensor can be determined from the slope of the current calibration curve in terms of concentration logarithm, which is equal to 157.85  $\mu\text{A}\mu\text{M}^{-1}\text{cm}^{-2}$ . Equation 7 was used to calculate the detection limit.

$$\text{LOD} = 3 \frac{SD}{m} \quad (7)$$

In which  $m$  is the slope of the calibration curve line and  $SD$  denotes the standard deviation. To calculate  $SD$ , a certain concentration of the control sample was measured under the same experimental conditions with three replications (5.79%). Accordingly, the detection limit of the designed biosensor was 0.035  $\mu\text{M}$ . The sensitivity and limit of detection of the designed biosensor are compared with other sensors as listed in Table 2.

### 3.10 Biosensor stability

Fig. S5 (See Supplemental Information) shows the cyclic voltammogram obtained from 25 consecutive repetitions of the cyclic voltammetry test under the mentioned conditions. As seen, after 25 consecutive cycles, a very small decrease can be detected in the current density peak, suggesting proper strength of the surface of the modified electrode against the applied potential.

### 3.11 Repeatability, stability and selectivity

To study the biosensor reproducibility, CF/CuO/Pt/CHO-MIP Nanocomposite attached on GCE was evaluated to measure a concentration of 0.8  $\mu\text{M}$  CHO in six repetitions. RSD of the designed biosensor was calculated to be 5.86% (Fig. 7A). Figure 7B shows the selectivity of the designed biosensor toward CHO in the presence of some interfering species (2  $\mu\text{M}$ ) such as glucose (Glu), ascorbic acid (AA), uric acid (UA), and dopamine (DA). Accordingly, the electrocatalytic behavior of the biosensor is distinctive in the presence of 4  $\mu\text{M}$  of CHO and other species caused minor disturbance in the current density of CHO. The stability of the designed biosensor over time was also evaluated; the biosensor managed to detect 4  $\mu\text{M}$  of CHO at 30-day intervals. Based on Fig. 7C, after 30 days, the biosensor response only decreased by 3% compared to its initial response. Therefore, it can be concluded that the designed electrode has good selectivity and can be used to monitor actual samples. Fig. S6 demonstrates a linear relationship between the current density and  $1/t^2$ . The CHO diffusion coefficient can be determined from the slope of this diagram, which is equal to  $7.8 \times 10^{-4}\text{cm}^2\text{s}^{-1}$ . Computational details of CHO diffusion coefficient are briefly described in the Supplemental Information.

**Table 2** Comparison of the response of some CHO biosensors with different types of electrodes

Number	Electrode	LOD	Linear range	Sensitivity	References
1	Cu/NiCNF/ACF/PMO	0.002 mg dL <sup>-1</sup>	0.04–600 mg dL <sup>-1</sup>	0.226 $\mu\text{A}\mu\text{M}^{-1}\text{cm}^{-2}$	[19]
2	ChOx/Au/ZnO/CNT	0.1 $\mu\text{M}$	0.1–100 $\mu\text{M}$	25.89 $\mu\text{A}\mu\text{M}^{-1}\text{cm}^{-2}$	[20]
3	Grp/ $\beta$ CD/Methylene Blue	0.1 mM	–	0.01 $\mu\text{A}\text{mM}^{-1}\text{cm}^{-2}$	[21]
4	Pt NP/(CNT)24 bilayer	–	0.005–10 mM	8.70 $\mu\text{A}\text{mM}^{-1}\text{cm}^{-2}$	[10]
5	Cu <sub>2</sub> S NRS	0.1 $\mu\text{M}$	0.01–6.8 mM	0.101 $\mu\text{A}\mu\text{M}^{-1}\text{cm}^{-2}$	[22]
6	Co(II)Cl <sub>2</sub> /Pt	2 $\mu\text{M}$	25–200 $\mu\text{M}$	7.32 $\mu\text{A}\text{mM}^{-1}\text{cm}^{-2}$	[23]
7	Cu <sub>2</sub> O NPs/TiO <sub>2</sub>	0.05 $\mu\text{M}$	24.4–622 $\mu\text{M}$	0.603 $\mu\text{A}\mu\text{M}^{-1}\text{cm}^{-2}$	[24]
8	PANI/MWCNTs/C MC/CPE	0.01 mM	0.05–5 mM	0.10 $\mu\text{A}\mu\text{M}^{-1}\text{cm}^{-2}$	[25]
9	$\beta$ -CD/MB/Gr	1 $\mu\text{M}$	1–100 $\mu\text{M}$	0.01 $\mu\text{A}\mu\text{M}^{-1}\text{cm}^{-2}$	[26]
10	CF/CuO/Pt-p-PD-CHO/MIP	0.035 $\mu\text{M}$	0.4–6 $\mu\text{M}$	157.85 $\mu\text{A}\mu\text{M}^{-1}\text{cm}^{-2}$	This work

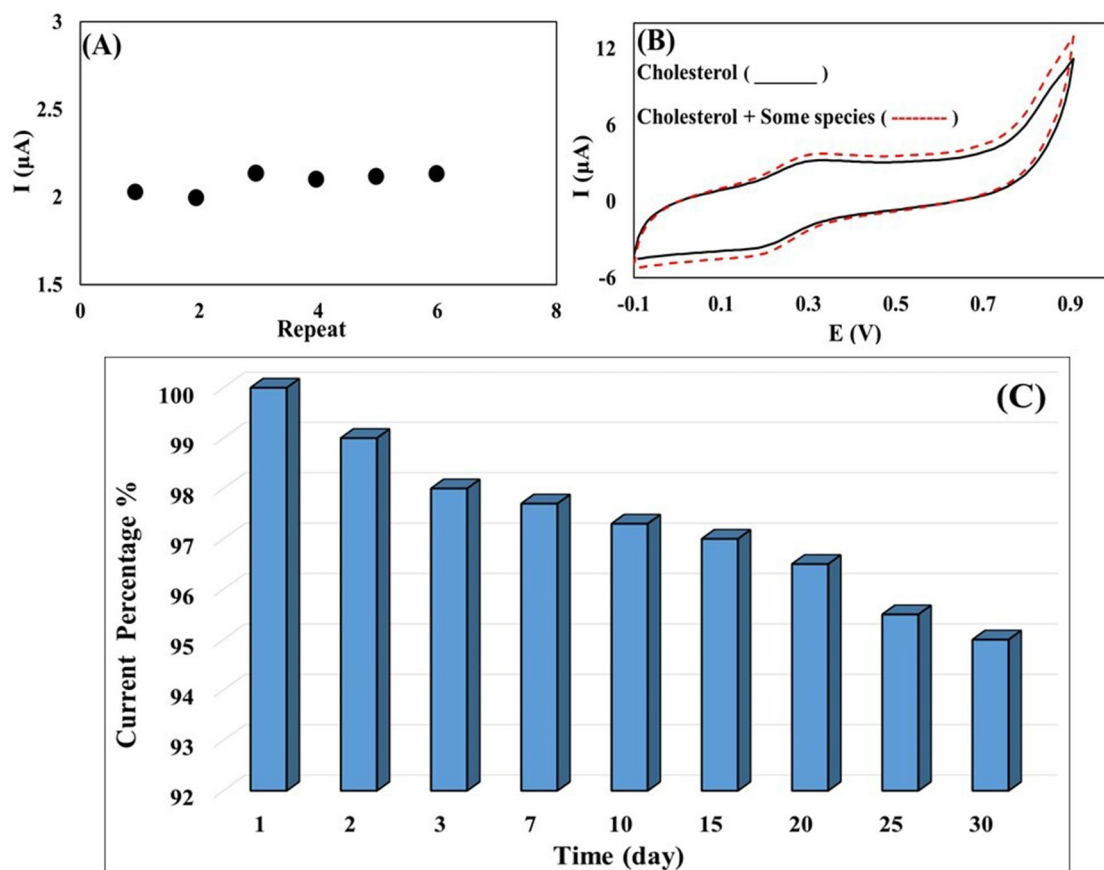


**Fig. 7** **A** The reproducibility of biosensor, **B** The diagram of CHO oxidation in the presence of 2  $\mu\text{M}$  some species such as glucose, ascorbic acid, uric acid and dopamine, **C** The diagram of biosensor stability over time. All solution were examined in the presence of 4  $\mu\text{M}$  of CHO

### 3.12 Artificial samples study

Non-enzymatic determination of cholesterol in real samples is a complex task due to the presence of different forms of cholesterol in biological matrices. For example, biological samples (mainly blood or serum) contain not only the free form of cholesterol, but also its esterified form. Therefore, esterified cholesterol should be first converted into the free state and then oxidized. However, to evaluate the practical applications of CF/CuO/Pt/CHO-p-PD biosensor, the artificial samples were collected from three healthy subjects. Artificial samples were diluted with phosphate buffer followed by adding known concentrations of cholesterol. Cholesterol solutions of different concentrations (0.8, 2 and 4  $\mu\text{M}$ ) were added to samples and recovery percentages were calculated. The recovery of 104.2% demonstrates the

applicability of the prepared CF/CuO/Pt/CHO-p-PD biosensor to real sample analysis.

## 4 Conclusion

A novel amperometric non-enzymatic CHO biosensor was developed based on electropolymerized para-phenylenediamine monomer as a molecularly imprinted polymer on copper foam modified with platinum and copper oxide (CuO) dual-core nanohybrid (CuO/Pt) attached on GCE. The activity of bimetallic nanoparticles with a polymer lattice was assessed to reach direct non-enzymatic electro-oxidation of CHO. The electrochemical behavior of the modified sensors was investigated and results indicated the significant catalytic activity of CF/CuO/Pt/

CHO-Molecular imprinted polymer for direct oxidation of CHO. A synergistic electro-catalytic effect was found between nanoparticles and polymeric lattice. Quantum chemistry and DFT numerical methods were used to reasonably and appropriately select the MIP and to achieve the best affinity between CHO and the monomers. The effect of CHO loading duration in MIP was investigated on biosensor response and time of 160 s was chosen as the optimal time for optimal loading of CHO molecules within the MIP structure. The fabricated sensors showed high sensitivity to CHO with acceptable selectivity even in the presence of interfering species. Therefore, application of CF/CuO/Pt, along with a suitable polymeric lattice (p-PD), leads to accurate, sensitive, and reliable modified electrodes which can be used for the non-enzymatic sensing of CHO.

**Supplementary Information** The online version contains supplementary material available at <https://doi.org/10.1007/s10800-023-01901-3>.

**Acknowledgements** The authors thank the INSF for funding the work; Project Code [98005610].

**Author contributions** FK and ME: wrote the main manuscript text and EJ, MS and AA: prepared all figures and tables. All authors reviewed the manuscript.

**Funding** Funding was provided by Iran National Science Foundation (Grant No. 98005610).

## Declarations

**Conflict of interest** The authors declare that they have no known competing financial interests or personal relationships that could have appeared to influence the work reported in this paper.

## References

- Polyakova I, Borovikova L, Osipenko A, Vlasova E, Volchek B, Pisarev O (2016) Surface molecularly imprinted organic-inorganic polymers having affinity sites for cholesterol. *React Funct Polym* 109:88–98
- Chung M, Jang YJ, Kim MI (2018) Convenient colorimetric detection of cholesterol using multi-enzyme co-incorporated organic-inorganic hybrid nanoflowers. *J Nanosci Nanotechnol* 18(9):6555–6561
- Thivya P, Ramya R, Wilson J (2020) Poly (3, 4-ethylenedioxythiophene)/taurine biocomposite on screen printed electrode: non-enzymatic cholesterol biosensor. *Microchem J* 157:105037
- Xia T, Liu G, Wang J, Hou S, Hou S (2021) MXene-based enzymatic sensor for highly sensitive and selective detection of cholesterol. *Biosens Bioelectron* 183:113243
- Mirzaei M, Behboudnia M, Kheiri F, Chianeh VA, Naeim H, Jannatdoust E, Sirousazar M (2019) Fabrication of non-enzymatic electrochemical hydrogen peroxide sensor based on Ag NPs/Co<sub>3</sub>O<sub>4</sub>/ERGO Composite. *J Electrochem Soc* 166(13):B1232
- Naeim H, Kheiri F, Sirousazar M, Afghan A (2018) Ionic liquid/reduced graphene oxide/nickel-palladium nanoparticle hybrid synthesized for non-enzymatic electrochemical glucose sensing. *Electrochim Acta* 282:137–146
- Molaei R, Sabzi RE, Farhadi K, Kheiri F, Forough M (2014) Amperometric biosensor for cholesterol based on novel nanocomposite array gold nanoparticles/acetone-extracted propolis/multi-wall carbon nanotubes/gold. *Micro & Nano Lett* 9(2):100–104
- Rajesh W, Takashima W, Kaneto K (2004) Amperometric tyrosinase based biosensor using an electropolymerized PTS-doped polypyrrole film as an entrapment support. *React Funct Polym* 59:163–169
- Li Y, Bai H, Liu Q, Bao J, Han M, Dai Z (2010) A nonenzymatic cholesterol sensor constructed by using porous tubular silver nanoparticles. *Biosens Bioelectron* 25(10):2356–2360
- Yang J, Lee H, Cho M, Nam J, Lee Y (2012) Nonenzymatic cholesterol sensor based on spontaneous deposition of platinum nanoparticles on layer-by-layer assembled CNT thin film. *Sens Actuators B Chem* 171:374–379
- Charan Ch, Shahi V (2014) Nanostructured manganese oxide-chitosan-based cholesterol sensor. *J Appl Electrochem* 44:953–962
- Kihal R, Fislil H, Chelaghmia M, Drissi W, Boukharouba C, Abdi S, Nacef M, Affoune A, Pontié M (2023) A novel and ultrasensitive non-enzymatic electrochemical glucose sensor in real human blood samples based on facile one-step electrochemical synthesis of nickel hydroxides nanoparticles onto a three-dimensional Inconel 625 foam. *J Appl Electrochem* 53:315–329
- Karasu T, Özgür E, Uzun L (2023) MIP-on-a-chip: artificial receptors on microfluidic platforms for biomedical applications. *J Pharm Biomed Anal* 226:115257
- Hong L, Liu A, Li G, Chen W, Lin X (2013) Chemiluminescent cholesterol sensor based on peroxidase-like activity of cupric oxide nanoparticles. *Biosens & Bioelect* 43:1–5
- Rafati Z, Sirousazar M, Hassan ZM, Kheiri F (2020) Honey-loaded egg white/poly (vinyl alcohol)/clay bionanocomposite hydrogel wound dressings: in vitro and in vivo evaluations. *J Polym Environ* 28(1):32–46
- Wang L, Kunsong L, Wenbao F, Chunyan C, Hang G, Changqun C (2021) Molecularly imprinted polymers based on magnetically fluorescent metal-organic frameworks for the selective detection of hepatitis A virus. *Microchem J* 164:106047–106054
- Roufegari-Nejhad E, Sirousazar M, Abbasi-Chiyaneh V, Kheiri F (2019) Removal of methylene blue from aqueous solutions using poly (vinyl alcohol)/montmorillonite nanocomposite hydrogels: Taguchi optimization. *J Polym Environ* 27(10):2239–2249
- Archana S, Jaya Shanthi R (2014) Synthesis and characterization of poly (p-phenylenediamine) in the presence of sodium dodecyl sulfate. *Res J Chem Sci* 2231:606X
- Bairagi PK, Verma N (2018) electrochemically deposited dendritic poly (methyl orange) nanofilm on metal-carbon-polymer nanocomposite: A novel non-enzymatic electrochemical biosensor for cholesterol. *J Electroanal Chem* 814(23):134–143
- Ghanei D, Darabi E, Elahi M (2020) Fabrication of Au/ZnO/MWCNTs electrode and its characterization for electrochemical cholesterol biosensor. *J Theor Appl Phys* 14:339–348
- Agnihotri N, Chowdhury AD, De A (2015) Non-enzymatic electrochemical detection of cholesterol using  $\beta$ -cyclodextrin functionalized graphene. *Biosens Bioelectron* 63:212–217
- Ji R, Wang LL, Wang GF, Zhang XJ (2014) Synthesize thickness copper (I) sulfide nanoplates on copper rod and its application as nonenzymatic cholesterol sensor. *Electrochim Acta* 130(5):239–244
- Thakur N, Gupta D, Mandal D, Nagaiah TC (2021) Ultrasensitive electrochemical biosensors for dopamine and cholesterol: recent advances, challenges and strategies. *Chem Commun* 57(97):13084–13113
- Khalique N, Rasheed MA, Cha G, Khan M, Karim SA, Schmuiki P, Ali G (2020) Development of non-enzymatic cholesterol

- bio-sensor based on TiO<sub>2</sub> nanotubes decorated with Cu<sub>2</sub>O nanoparticles. *Sens. Actuator B-Chem* 302(43):127200
25. Lakshmi G, Sharma A, Solanki PR, Avasthi DK (2016) Mesoporous polyaniline nanofiber decorated graphene microflowers for enzyme-less cholesterol biosensors. *Nanotechnology* 27(34):323–329
26. Tong YJ, Li HD, Guan HM, Zhao JM, Majeed S, Anjum S, Liang F, Xu GB (2013) Electrochemical cholesterol sensor based on carbon nanotube@molecularly imprinted polymer modified ceramic carbon electrode. *Biosens Bioelectron* 47(32):553–558

**Publisher's Note** Springer Nature remains neutral with regard to jurisdictional claims in published maps and institutional affiliations.

Springer Nature or its licensor (e.g. a society or other partner) holds exclusive rights to this article under a publishing agreement with the author(s) or other rightsholder(s); author self-archiving of the accepted manuscript version of this article is solely governed by the terms of such publishing agreement and applicable law.

## Authors and Affiliations

Milad Eghbali<sup>1,2</sup> · Farshad Kheiri<sup>3</sup> · Mohammad Sirousazar<sup>1</sup> · Elham Jannatdoust<sup>1</sup> · Arash Afghan<sup>3</sup>

✉ Farshad Kheiri  
F.Kheiri@uut.ac.ir

<sup>1</sup> Faculty of Renewable Energy, Department of Chemical Engineering, Urmia University of Technology, Urmia, Iran

<sup>2</sup> Institute of Biotechnology, Urmia University, Urmia, Iran

<sup>3</sup> Faculty of Renewable Energy, Department of Applied Chemistry, Urmia University of Technology, Urmia P.O. Box 57155-419, West Azerbaijan, Iran